



GPS constraints on 34 slow slip events within the Cascadia subduction zone, 1997–2005

W. Szeliga,^{1,2} T. Melbourne,¹ M. Santillan,¹ and M. Miller¹

Received 22 January 2007; revised 15 October 2007; accepted 27 December 2007; published 8 April 2008.

[1] Refinements to GPS analyses in which we factor geodetic time series to better estimate both reference frames and transient deformation resolve 34 slow slip events located throughout the Cascadia subduction zone from 1997 through 2005. Timing of transient onset is determined with wavelet transformation of geodetic time series. Thirty continuous stations are included in this study, ranging from northern California to southwestern British Columbia. Our improvements in analysis better resolve the largest creep events and also identify many smaller events. At 48.5°N latitude, a 14-month average recurrence interval has been observed over eight events since 1997. Farther north along Vancouver Island a host of smaller events with a distinct 14-month periodicity also occurs. In southern Washington State, some of the largest transient displacements are observed but lack any obvious periodicity in their recurrence. Along central Oregon, an 18-month recurrence is evident, while in northern California an 11-month periodicity continues through 2005. We invert GPS offsets of the 12 best recorded events for thrust slip along the plate interface using a cross-validation scheme to derive optimal smoothing parameters. These 12 events have equivalent moment magnitudes between 6.3 and 6.8 and have 2–3 cm of slip. Unlike other subduction zones, no long-duration events are observed, and cumulative surface deformation is consistently less than 0.6 cm. The many newly resolved smaller transient events in Cascadia show that slow slip events occur frequently with GPS best capturing only the largest events. It is likely that slow slip events occur more frequently at levels not detectable with GPS.

Citation: Szeliga, W., T. Melbourne, M. Santillan, and M. Miller (2008), GPS constraints on 34 slow slip events within the Cascadia subduction zone, 1997–2005, *J. Geophys. Res.*, 113, B04404, doi:10.1029/2007JB004948.

1. Introduction

[2] Over the past decade, continuous geodetic measurements above subduction zones have revealed a range of transient deformation consistent with creep along the deeper plate interface. Early GPS and borehole strainmeter transients offshore Japan were inferred to be slow slip episodes [Hirose *et al.*, 1999; Kawasaki *et al.*, 1995] but appeared, because of instrumentation limitations, as isolated occurrences. The ongoing proliferation of GPS, however, has afforded their routine detection both in Japan and elsewhere [Larson *et al.*, 2004; Lowry *et al.*, 2001; Ohta *et al.*, 2006; Ozawa *et al.*, 2002]. In Cascadia, the initial recognition with GPS of transient slow faulting along the megathrust [Dragert *et al.*, 2001] led to identification of eight additional events with a regular, 14.5 ± 1 month periodicity [Miller *et al.*, 2002] and the forecasting of future events, four of which have occurred to date with the same period-

icity. It was originally assumed these events release large amounts of strain energy without detectable seismic shaking, but independent confirmation of Cascadia events came jointly from the discovery of subduction-related tremor signals in Japan [Obara, 2002] and their subsequent correlation in Cascadia with GPS-inferred slow slip events [Rogers and Dragert, 2003]. Subsequent analysis of GPS from elsewhere in Cascadia shows that the slow slip events, also known as episodic tremor and slip (ETS [after Rogers and Dragert, 2003]) likely occur throughout the Cascadia subduction zone, including beneath northern California, with a different and distinctive 10.9 ± 1.2 month periodicity, and offshore central Oregon with a 18 ± 2 month periodicity [Szeliga *et al.*, 2004]. Analyses of seismic tremor from the region support these GPS-based inferences [Kao *et al.*, 2005; McCausland *et al.*, 2005] and show that many smaller events occur beneath what is detectable with GPS.

[3] The mechanism by which slow slip occurs remains uncertain at the present time, and in particular, whether creep occurs in the absence of detectable seismicity, simultaneous with seismicity, or not at all, meaning measured surface deformation represents the integrated deformation from a large number of discrete, seismic slip events, has not yet been determined. Depth estimations from both Cascadia and Japan show epicentral locations that consistently overlie the 25 to 40 km depth contours and 350°F isotherm of the

¹Department of Geological Sciences, Central Washington University, Ellensburg, Washington, USA.

²Now at the Department of Geological Sciences, University of Colorado, Boulder, Colorado, USA.

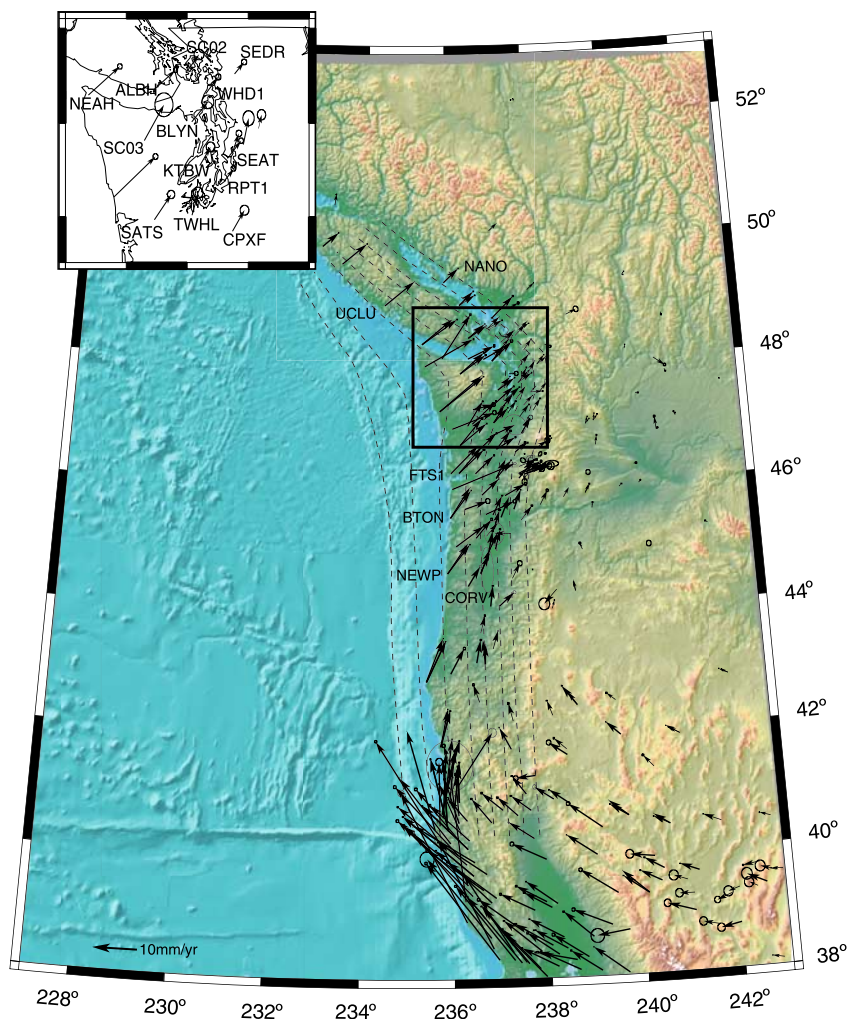


Figure 1. Interseismic deformation from 1997.0 through 2006.0 from the Cascadia subduction zone. Stations with labels show transient deformation associated with slow slip along the Juan de Fuca–North American plate interface. Coastal stations show smaller transients due to their larger radial distance from the location of transient creep. Velocities are relative to stable North America as realized by SNARF Version 1.0.

subducted plate [Kao *et al.*, 2005; McCausland *et al.*, 2005; Obara, 2002], suggesting eclogitic dehydration-derived fluids may play a role in promoting transient slip. Complicating this picture are tremor hypocentral depth estimates in Cascadia, which appear over a 40 km vertical range centered around the plate boundary [Kao *et al.*, 2005; McCausland *et al.*, 2005; Obara, 2002; Royle *et al.*, 2006]. These depths imply that either tremor sources, and presumably slip, are spread radially over a wide range, or unmodeled diffraction of high frequency tremor (typically 1–6 Hz) bias the depth estimates. Along the Nankai Trough in Japan, however, hypocentral locations of very low frequency events that occur simultaneously with tremor both locate to the subducting plate interface [Ide *et al.*, 2007; Ito *et al.*, 2007; Shelly *et al.*, 2006] and show thrust fault mechanisms [Ide *et al.*, 2007]. These inferences suggest, as of the present time, that tremor originates from impulsive thrust slip sources along the plate interface and are not likely scattered radially.

[4] GPS deformation is insensitive to the details of slip and cannot resolve the source process. However, it is currently the

sole method for constraining the total equivalent moment of slip for a given episode of tremor, which eludes seismic and strainmeter analysis at the present time. Since transient plate interface slip impacts the developing moment budget, either by reducing the size of a future earthquake or delaying its recurrence, it is worthwhile to systematically document the sizes and characteristics of known slow slip events inferable from existing geodetic measurements. In Cascadia, fore-arc crustal deformation is dominated by subduction related strain accumulation (Figure 1), but improvements to processing show that 34 events of variable frequency and magnitude occurred from 1997 through 2005, and that these events show a wide variety of cyclical and aperiodic strain release.

2. GPS Data Analysis

[5] All data were initially point positioned with the GIPSY-OASIS software [Zumberge *et al.*, 1997], yielding scatter typically around 1 cm (Figure 2a).

[6] Although this method works well enough for determining long-term tectonic rates, it is insufficient

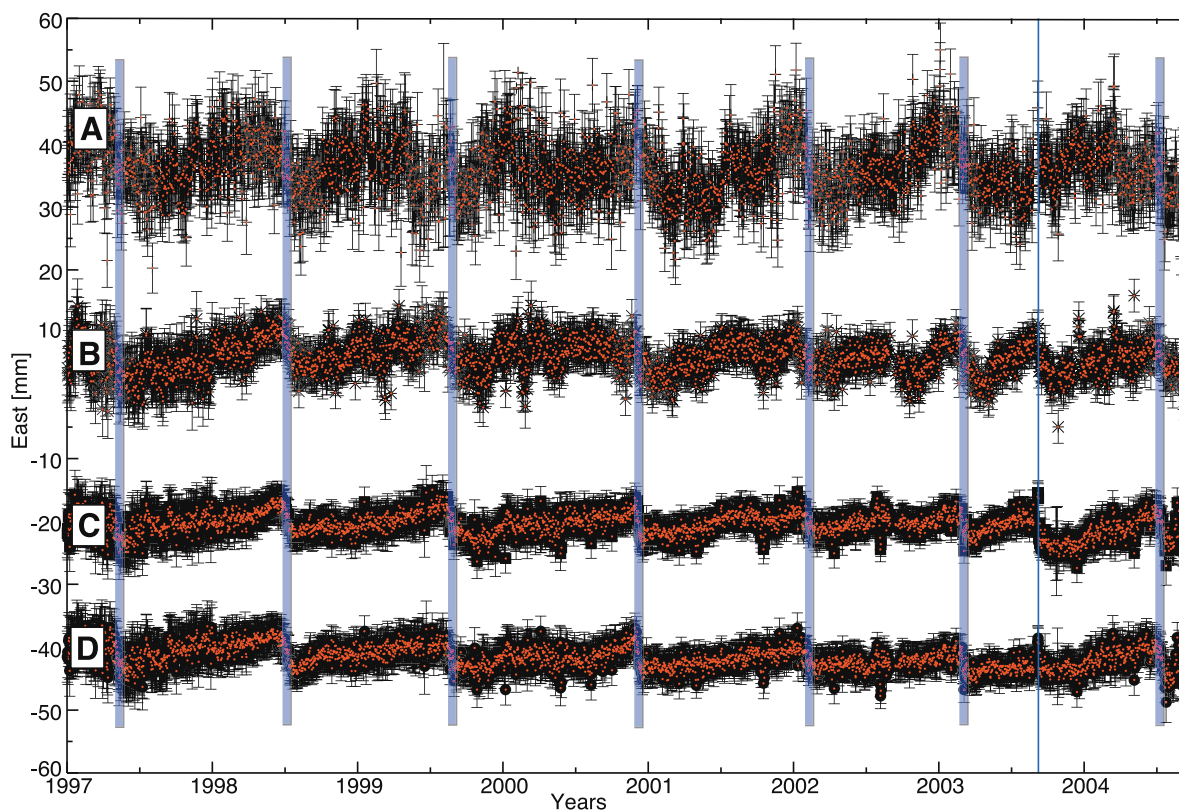


Figure 2. Successive levels of GPS data analysis used to refine estimates of slow slip events. All plots show the longitude component of station ALBH (Figure 1). (a) Point positioning; (b) network analysis with biases solved by differencing; (c) bias-resolved network analysis stabilized to Pacific Northwest dominated average positions; (d) time series reconstructed from basis functions decomposed in both network stabilization and postprocessing steps. Basis functions are shown in Figure 3. Vertical lines indicate times of known slow slip events.

for constraining the subtle transients indicative of slow earthquakes. Biases are then resolved using the method of *Blewitt* [1989]. This solution (Figure 2b) is then transformed into ITRF2000 using daily frame data products provided by the International Geodynamics Service [Zumberge *et al.*, 1997]. The last formal GIPSY processing step is to regionally stabilize the PANGA network by applying a transformation to each daily position. This final stabilization entails using a reference set of 42 stations from the North America plate region, of which 23 of these are concentrated in the Pacific Northwest and the remainders are distributed on the stable North American plate interior or in other regional networks in western North America [Miller *et al.*, 2001]. Of the 42 stations, 33 have published positions and velocities in ITRF2000. This stabilization transformation serves to minimize networkwide position discrepancies and common mode errors while still recovering all differential motion of the Cascadia fore arc and back arc relative to stable North America (Figure 2c).

[7] In both the process of estimating linear plate tectonic motion in establishing the reference frame as well as for extracting transient deformation signals, it is necessary to estimate and remove seasonal effects known to contaminate GPS time series [Blewitt and Lavallée, 2002; Dong *et al.*, 2002; Mao *et al.*, 1999], as well as other sources of error.

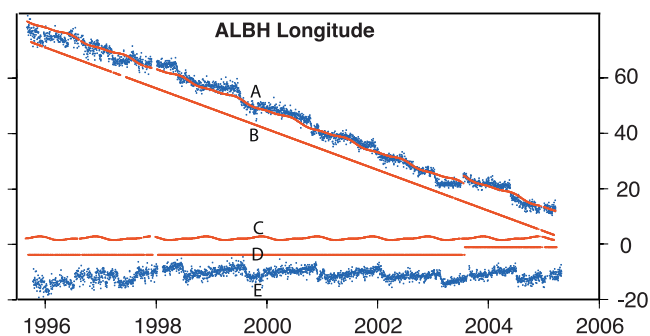


Figure 3. Factorization of raw geodetic time series (A) takes place in reference frame estimations and postprocessing. Time series are factored with QR decomposition into a linear trend (B) a summation of annual and semiannual sinusoidal signals which are assumed to have stationary phase (C), and a summation of step functions corresponding to times of known hardware changes (D) (derived from metadata). Once these known signals are removed, a time series showing the geodetic signature of slow slip events remains (E). Onset times for each slow slip event are selected using a wavelet transform (Figure 4).

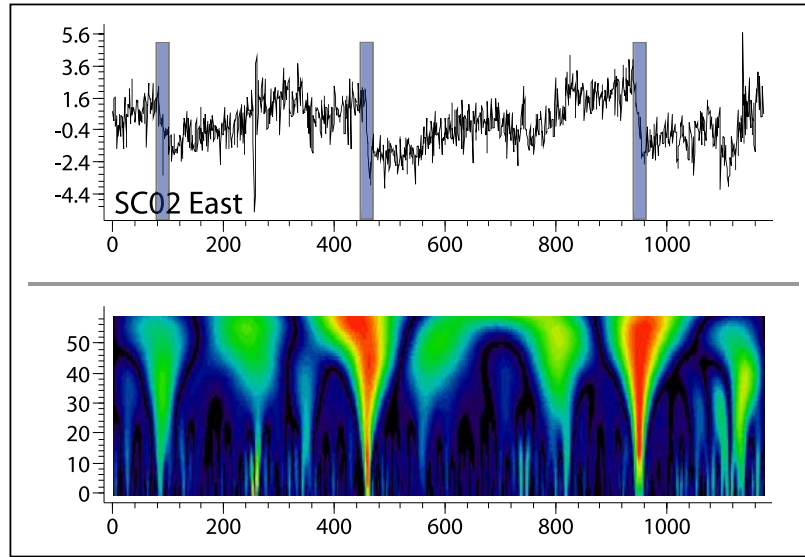


Figure 4. (top) Wavelet transform used for picking onset times applied to the longitude component of stations SC02. (bottom) Vertical scale shows degree of temporal localization of transient signal; since slow slip events produce permanent deformation they extend across all temporal scales and their times can be picked by assessing the time at the most localized temporal scale.

Geodetic time series are therefore decomposed into discrete basis functions represented by the following functional:

$$y(t_i) = a + bt_i + \sum_j c'_j \sin(f_j t_i + d'_j) + \sum_k e'_k H(t_i - T_k), \quad (1)$$

where $H()$ is the Heaviside function, a is site position, b is the site velocity, c'_j , d'_j are the amplitudes and phases of the j th sinusoidal signals with frequencies f_j , and e'_k are discrete steps or earthquakes occurring at epochs T_k . The unknowns $a - e'_k$ may be considered as the scaling factors of basis functions into which GPS time series may be decomposed. Some time series require additional basis functions to fully describe the behavior of the station, such as those exhibiting logarithmic decay of postseismic transients, but those are isolated cases and not generally included in routine processing. More commonly, site maintenance involves removal of GPS antennas or installation of radomes, resulting in the introduction of discrete steps with the same functional form as earthquakes. These discrete steps may be estimated and removed from time series through the addition of the last basis function in equation (1). Figure 3 shows this decomposition for the longitude component of station ALBH, with each blue dot showing a daily solution.

[8] Estimation of motion during a slow slip event proceeds by masking out data during the slow slip event and estimating the resulting offset by appending additional basis functions to equation (1) of the form,

$$\sum_l g'_l H(t_i - T_l),$$

where g'_l are the amplitudes of the slow slip events at epoch T_l .

[9] For time series that do not contain offsets, straightforward application of trigonometric addition formulas to equation (1) yields

$$y(t_i) = a + bt_i + c \sin\left(\frac{2\pi}{\tau} t_i\right) + d \cos\left(\frac{2\pi}{\tau} t_i\right) + e \sin\left(\frac{4\pi}{\tau} t_i\right) + f \cos\left(\frac{4\pi}{\tau} t_i\right). \quad (2)$$

Here a and b are as in equation (1), while combinations of c and d describe an annual signal, e and f describe a semiannual signal and τ is the period. Since equation (2) is linear in the unknowns $a-f$ we may form the matrix:

$$A = \begin{pmatrix} 1 & t_0 & \sin\left(\frac{2\pi}{\tau} t_0\right) & \cos\left(\frac{2\pi}{\tau} t_0\right) & \sin\left(\frac{4\pi}{\tau} t_0\right) & \cos\left(\frac{4\pi}{\tau} t_0\right) \\ \vdots & \vdots & \vdots & \vdots & \vdots & \vdots \\ 1 & t_n & \sin\left(\frac{2\pi}{\tau} t_n\right) & \cos\left(\frac{2\pi}{\tau} t_n\right) & \sin\left(\frac{4\pi}{\tau} t_n\right) & \cos\left(\frac{4\pi}{\tau} t_n\right) \end{pmatrix},$$

where n is the number of GPS position observations. Equation (2) may now be rewritten in matrix-vector form as

$$y = Ax + r, \quad (3)$$

where x is a vector consisting of the unknowns $a-f$, y is a vector consisting of GPS position observations and r is a vector of residuals. Solution of the system of equations (3) proceeds by forming the weighted normal equations with weight matrix C consisting of the inverse covariances of the observations y :

$$A^T C A x = A^T C y, \quad (4)$$

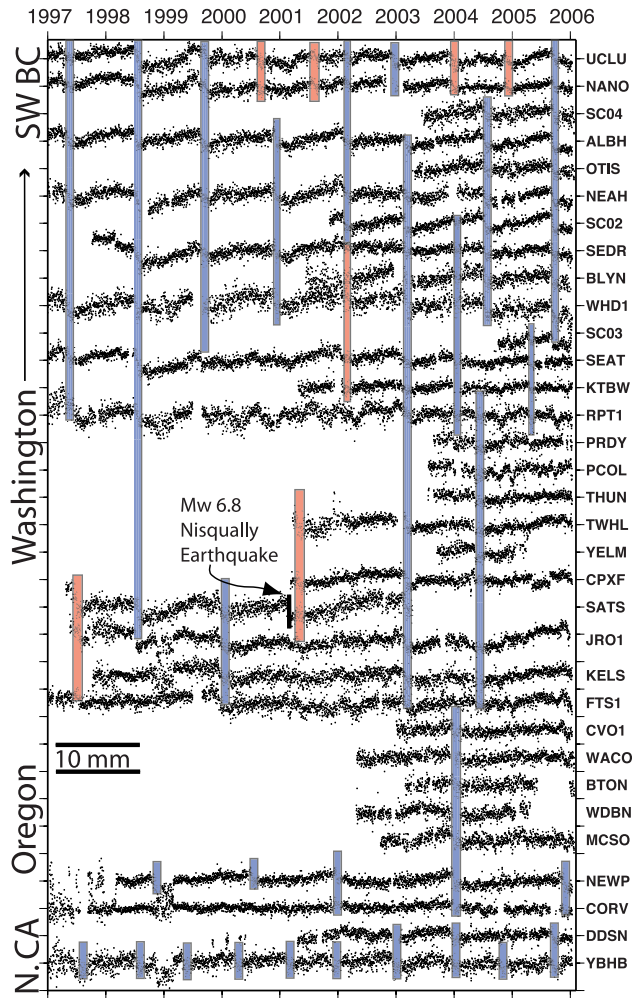


Figure 5. Nine years of GPS longitude measurements from the Cascadia subduction zone show evidence of over 30 slow slip events localized throughout the convergent margin. Vertical tick marks are 10 mm. Blue boxes indicate slip events either well recorded with GPS or corroborated by observations of subduction zone tremor. Red lines indicate spatially coherent transient GPS deformation typical of slow slip events but recorded on less than four stations and uncorroborated at this time by tremor. Maximum geodetic offsets are 6 mm and correspond to the spatially largest event in early 2003; the smallest discernible events show 2 mm of deformation. Horizontal deformation for the 12 largest transients is shown in Figure 7. Offset from the February 2001, Nisqually earthquake appears only on station SATS, which is closest to the epicenter.

where A^t denotes the matrix transpose of A . Following Nikolaidis [2002] we achieve the best linear unbiased estimate of the vector x , by using the QR decomposition of equation (4). Equation (4) then becomes

$$\hat{x} = R^{-1}Q^tA^tCy, \quad (5)$$

where $QR = A^tCA$. Computationally, QR decomposition is more numerically stable than explicitly inverting the weighted normal equations (5). By defining the residual time series as $\hat{r} = y - A\hat{x}$, we may then propagate covariances

forward to yield covariances (Σ) for the unknowns, modeled observations and residuals,

$$\begin{aligned} \sigma_0^2 &= \frac{r^tCr}{n - m}, \\ \Sigma_{\hat{x}} &= \sigma_0^2(A^tCA)^{-1}, \\ \Sigma_{A\hat{x}} &= \sigma_0^2A(A^tCA)^{-1}A^t, \\ \Sigma_{\hat{r}} &= \sigma_0^2(C^{-1} - A(A^tCA)^{-1}A^t). \end{aligned} \quad (6)$$

In equation (6), m is the number of basis functions used in the decomposition and n is the number of observations. Decomposition of equation (6) is performed using a Householder QR algorithm (Algorithm 5.2.1 [Golub and Val Loan, 1996]). The decomposition allows basis functions (Figure 3) to be modeled individually or added back to residuals; Figure 2d shows the ALBH residuals, which for most stations are largely white noise, with only the slow slip offsets added back. All selected PANGA time series after filtering are shown in Figure 4.

[10] One drawback to this approach is that the timing of the slow slip events needs to be specified independently, as do hardware upgrade times (these are obtained from GPS

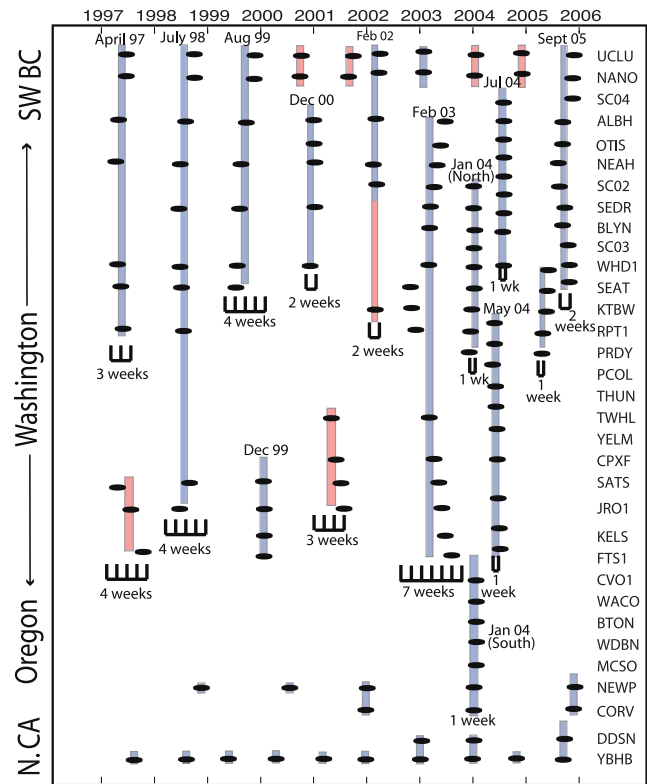


Figure 6. Temporal evolution of slow slip events identified from time picks of transient deformation. Most events last 3–4 weeks, propagate at average rates of 10–15 km/d and are observed to propagate both unidirectionally and bidirectionally. While typical durations are 3–4 weeks, the shortest and longest events are 1 week and 7 weeks, respectively. Longer-duration events with larger amplitudes, which have been observed in other subduction zones, are not observed in the Cascadia subduction zone.

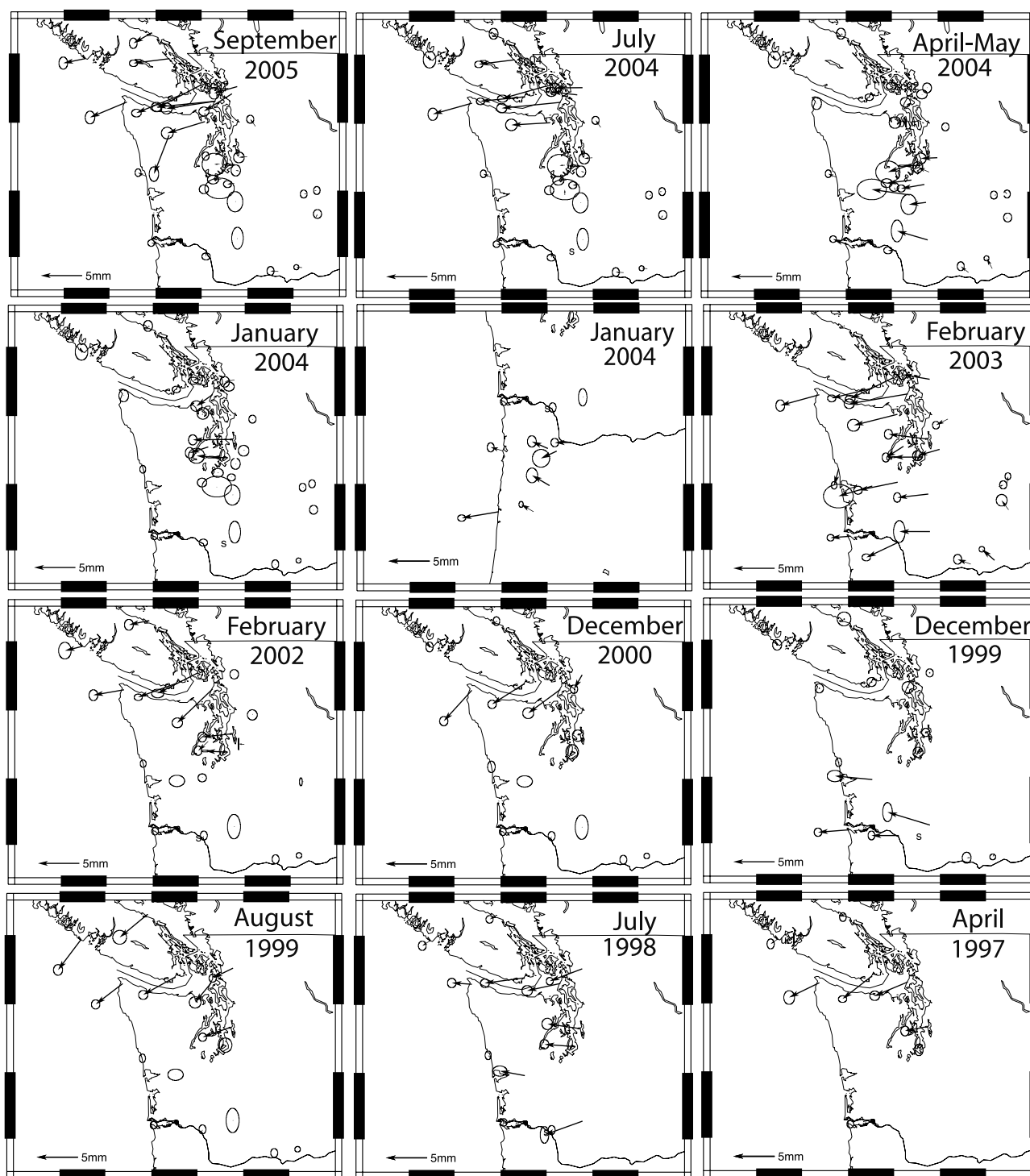


Figure 7. Cumulative surface deformation from the 12 best resolved slow slip events since 1997. See Figure 1 for station names.

station metadata). For Cascadia, identification of creep onset times with GPS can be difficult due to the low signal-to-noise ratio of the measurements. To make estimation of onset times repeatable, we use a Gaussian wavelet transform to identify initiation of slip. This approach employs the fact that succeeding wavelet basis functions are increasingly sensitive to temporal localization of any given signal, unlike the periodic sinusoids of the Fourier transform. Slow faulting at depth, which effectively produces a Heaviside step at

the onset of faulting, appears in the wavelet transform as an amplitude spike that pervades the wavelet power spectrum (Figure 5).

[11] Faulting initiation is precisely identified from the temporal location of this spike in amplitudes of wavelets with greatest localization. Besides being less prone to human or reference frame biases, the wavelet transform also allows clear discrimination of slow faulting deformation from other transient, nonsolid earth signals such as

Table 1. Measured Cumulative Transient Deformation for the 12 Best Detected Events Along the Cascadia Subduction Zone From 1997 Through 2005^a

Station	Station					
	Latitude	Longitude	Δ North	σ North	Δ East	σ East
<i>September 2005</i>						
UCLU	48.93	-125.54	-0.54	0.30	-2.59	0.22
NEAH	48.30	-124.62	-1.86	0.32	-4.45	0.24
ALBH	48.39	-123.49	-2.08	0.19	-5.16	0.24
SC04	48.92	-123.70	-0.54	0.16	-4.31	0.20
SC02	48.55	-123.01	-2.80	0.17	-5.34	0.24
SC03	47.82	-123.71	-4.70	0.36	-1.83	0.23
BLYN	48.02	-122.93	-1.39	0.29	-4.54	0.29
SEDR	48.52	-122.22	-0.79	0.29	-2.79	0.25
OTIS	48.42	-122.34	-2.12	0.22	-3.40	0.25
WHD1	48.31	-122.70	-0.89	0.27	-5.92	0.28
KTBW	47.55	-122.80	-0.31	0.21	-0.64	0.17
NANO	49.29	-124.09	-1.27	0.26	-2.21	0.19
LKCP	47.94	-121.83	0.87	0.20	-0.61	0.18
PABH	47.21	-124.20	0.42	0.19	-0.98	0.15
WHD1	48.31	-122.70	-0.71	0.23	-7.14	0.25
<i>July 2004</i>						
NANO	49.29	-124.09	0.02	0.27	-0.40	0.22
NEAH	48.30	-124.62	-1.33	0.30	-4.75	0.24
ALBH	48.39	-123.49	-0.54	0.16	-5.31	0.20
SC04	48.92	-123.70	-0.54	0.16	-4.31	0.20
BLYN	48.02	-122.93	-0.27	0.28	-4.68	0.29
SC02	48.55	-123.01	-1.51	0.17	-5.31	0.25
SEDR	48.52	-122.22	-0.02	0.24	-3.34	0.22
OTIS	48.42	-122.34	0.37	0.22	-3.14	0.26
LKCP	47.94	-121.83	0.87	0.20	-0.61	0.18
PABH	47.21	-124.20	0.42	0.19	-0.98	0.15
WHD1	48.31	-122.70	-0.71	0.23	-7.14	0.25
<i>April–May 2004</i>						
PUPU	47.50	-122.01	-0.08	0.26	-1.99	0.26
RPT1	47.39	-122.37	-0.05	0.03	-2.12	0.24
PABH	47.21	-124.20	0.42	0.19	-0.98	0.15
PRDY	47.39	-122.61	-0.83	0.54	-2.64	0.60
ZSE1	47.29	-122.19	0.59	0.28	-1.38	0.23
PCOL	47.17	-122.57	-0.38	0.21	-3.00	0.28
THUN	47.11	-122.29	-0.49	0.17	-2.82	0.20
CPXF	46.84	-122.26	-0.25	0.50	-2.08	0.38
FTS1	46.20	-123.96	0.66	0.16	-1.77	0.17
YELM	46.95	-122.61	0.67	0.51	-4.61	0.73
KELS	46.12	-122.90	0.00	0.17	-1.03	0.21
JRO1	46.28	-122.22	1.09	0.54	-3.70	0.28
<i>January 2004 (North)</i>						
SC02	48.55	-123.01	-0.29	0.17	-0.64	0.25
SEDR	48.52	-122.22	-0.22	0.26	-1.18	0.23
WHD1	48.31	-122.70	-1.41	0.26	-1.98	0.28
SEAT	47.65	-122.31	-0.04	0.25	-4.57	0.21
KTBW	47.55	-122.80	-0.72	0.26	-2.24	0.21
RPT1	47.39	-122.37	0.06	0.04	-1.99	0.24
PRDY	47.39	-122.61	0.20	0.37	-2.45	0.40
<i>January 2004 (South)</i>						
CHZZ	45.49	-123.98	0.41	0.21	-1.43	0.17
WACO	45.52	-122.99	0.82	0.27	-1.95	0.22
BTON	45.49	-122.80	-0.85	0.42	-1.91	0.43
MCSO	44.97	-122.96	1.19	0.35	-2.12	0.28
CVO1	45.61	-122.50	-0.02	0.20	-1.93	0.19
NEWP	44.59	-124.06	-0.72	0.15	-4.47	0.20
CORV	44.59	-123.30	0.86	0.14	-1.50	0.11
<i>February 2003</i>						
UCLU	48.93	-125.54	-0.60	0.23	-0.89	0.19
NEAH	48.30	-124.62	-1.30	0.28	-4.72	0.22
ALBH	48.39	-123.49	-1.19	0.17	-4.82	0.20
SC00	46.95	-120.73	0.20	0.20	0.56	0.18
SC02	48.55	-123.01	-2.55	0.17	-5.25	0.24
PABH	47.21	-124.20	-1.98	0.18	-0.54	0.14

Table 1. (continued)

Station	Station					
	Latitude	Longitude	Δ North	σ North	Δ East	σ East
WHD1	48.31	-122.70	-1.20	0.24	-7.10	0.25
JRO1	46.28	-122.22	0.01	0.54	-3.70	0.28
TWHL	47.02	-122.92	-0.98	0.20	-4.78	0.21
SATS	46.96	-123.47	-1.22	0.58	-4.09	0.73
CPXF	46.84	-122.26	-0.43	0.23	-3.74	0.18
FTS1	46.20	-123.96	-0.18	0.16	-2.36	0.17
KELS	46.12	-122.90	0.00	0.17	-3.93	0.21
GOBS	45.84	-120.81	1.35	0.14	-1.53	0.14
GWEN	45.78	-121.33	0.58	0.24	-1.60	0.20
YAWA	46.60	-120.51	1.14	0.29	-0.85	0.27
BLYN	48.02	-122.93	-1.33	0.29	-5.28	0.30
SEDR	48.52	-122.22	0.57	0.24	-3.29	0.21
KTBW	47.55	-122.80	-1.36	0.22	-2.13	0.18
SEAT	47.65	-122.31	0.57	0.24	-4.51	0.20
PUPU	47.50	-122.01	-0.76	0.24	-2.67	0.24
RPT1	47.39	-122.37	-0.01	0.02	-3.53	0.20
LKCP	47.94	-121.83	-0.73	0.19	-1.42	0.17
<i>February 2002</i>						
UCLU	48.93	-125.54	-0.51	0.41	-2.05	0.31
NANO	49.29	-124.09	-0.52	0.27	-2.40	0.22
ALBH	48.39	-123.49	-1.66	0.16	-4.60	0.20
NEAH	48.30	-124.62	-0.64	0.27	-3.70	0.22
SC02	48.55	-123.01	-2.51	0.21	-4.92	0.30
WHD1	48.31	-122.70	-4.10	0.24	-4.28	0.26
KTBW	47.55	-122.80	-1.14	0.23	-1.21	0.19
SEAT	47.65	-122.31	-0.36	0.24	-3.42	0.21
PUPU	47.50	-122.01	0.06	0.30	-0.70	0.22
RPT1	47.39	-122.37	0.13	0.04	-2.67	0.21
<i>December 2000</i>						
NEAH	48.30	-124.62	-3.71	0.23	-3.38	0.21
ALBH	48.39	-123.49	-2.45	0.21	-3.86	0.21
SEDR	48.52	-122.22	-1.71	0.21	-0.99	0.18
WHD1	48.31	-122.70	-2.87	0.27	-3.89	0.27
RPT1	47.39	-122.37	0.10	0.35	-0.37	0.31
<i>December 1999</i>						
RPT1	47.39	-122.37	-0.22	0.25	-0.56	0.24
SATS	46.96	-123.47	0.43	0.28	-4.50	0.38
FTS1	46.20	-123.96	-0.30	0.20	-3.87	0.19
KELS	46.12	-122.90	0.00	0.22	-3.30	0.17
JRO1	46.28	-122.22	1.57	0.47	-5.13	0.24
GOBS	45.84	-120.81	-0.36	0.14	-0.21	0.14
GWEN	45.78	-121.33	-0.02	0.27	-0.51	0.22
<i>August 1999</i>						
NEAH	48.30	-124.62	-2.50	0.23	-3.26	0.21
ALBH	48.39	-123.49	-2.12	0.22	-3.83	0.23
SEDR	48.52	-122.22	-1.19	0.20	-2.46	0.18
WHD1	48.31	-122.70	-2.38	0.28	-1.96	0.29
SEAT	47.65	-122.31	-1.13	0.20	-3.20	0.20
UCLU	48.93	-125.54	-3.59	0.26	-2.71	0.22
NANO	49.29	-124.09	-2.77	0.34	-3.35	0.34
<i>July 1998</i>						
UCLU	48.93	-125.54	-0.60	0.23	-0.89	0.19
NANO	49.29	-124.09	-0.53	0.19	-0.85	0.18
NEAH	48.30	-124.62	0.17	0.23	-2.42	0.21
ALBH	48.39	-123.49	-0.63	0.21	-4.75	0.22
SEDR	48.52	-122.22	-1.48	0.19	-3.93	0.17
WHD1	48.31	-122.70	-0.88	0.25	-4.03	0.26
SEAT	47.65	-122.31	0.55	0.28	-3.74	0.27
RPT1	47.39	-122.37	0.28	0.23	-3.73	0.22
PABH	47.21	-124.20	0.37	0.21	-0.36	0.15
SATS	46.96	-123.47	0.55	0.25	-3.01	0.36
FTS1	46.20	-123.96	0.41	0.18	0.14	0.17
JRO1	46.28	-122.22	-1.66	0.41	-4.60	0.21
<i>April 1997</i>						
UCLU	48.93	-125.54	-0.56	0.25	-0.79	0.18
NANO	49.29	-124.09	-0.44	0.21	-0.14	0.16

Table 1. (continued)

Station	Station		Δ North	σ North	Δ East	σ East
	Latitude	Longitude				
NEAH	48.30	-124.62	-1.77	0.34	-3.64	0.26
ALBH	48.39	-123.49	-2.73	0.16	-3.51	0.20
WHD1	48.31	-122.70	-1.68	0.23	-4.02	0.24
SEAT	47.65	-122.31	-0.48	0.24	-2.52	0.20
RPT1	47.39	-122.37	-0.59	0.28	-0.47	0.20

^aUnits are in millimeters, errors are 2σ .

those that arise from colored noise [Langbein and Johnson, 1997; Torrence and Compo, 1998]. Furthermore, times picked from the wavelet transform produce a significant reduction in chi-square misfits in event offset parameter estimation, at least for short-duration transients lasting less than two weeks. The output of transient onset times is used to estimate the propagation of transient deformation along strike (Figure 6) and cumulative vector offsets for each event (Figure 7 and Table 1).

3. Cascadia Slow Slip Events

[12] The filtered GPS longitude time series (Figure 4) highlight the variable style and recurrence of Cascadia slow slip events resolvable with GPS, as do the vector offsets estimated for the individual events (Figure 7). The 14-month periodicity identified by Miller *et al.* [2002] is primarily confined to northwestern Washington and southwestern British Columbia near the latitude of 48.5°N ; to the north and south this periodicity is not obvious. Some but not all events propagate up to the latitude 49°N (events in 1997, 1998, 1999, 2002, 2005), others are confined specifically to the region near the Strait of Juan de Fuca, while others propagate to the south from this region (1998, 2003). The spatial distribution of deformation transients, even for the region of regular 14-month recurrence, is thus quite variable. During some events, such as 1998 and 2003, rupture occurs to the north and south of the Straits of Juan de Fuca region, while during other events, such as the 2000 and 2004.5, are confined to the Puget Sound area. Interspersed throughout this area are numerous smaller events, such as 2004.0 and 2005.3, which occur out of sequence but with smaller magnitude than the 14-month events. To the north, central Vancouver Island shows smaller, isolated events of lower amplitude with no obvious periodicity; recurrence times for smaller events here range from 7 to 15 months. For northernmost Vancouver Island, another 14-month periodicity has been documented by Dragert *et al.* [2004], but here the events are 6 months out of phase with events in the Straits of Juan de Fuca.

[13] South of the Straits of Juan de Fuca, the 14-month periodicity disappears. Six events occur between 46°N and 48°N (Portland, Oregon, to Seattle, Washington), with recurrence ranging from 1.5 to 3 years. The instrumentation here is generally sparser than to the north, thus it is likely that many events have gone undetected prior to 2003.

[14] Central Oregon shows an 18-month periodicity, as documented previously by Szeliga *et al.* [2004], with the most recent event having occurred in late 2005. Interestingly, here the coastal site at Newport, Oregon, shows greater amplitudes of offset than the site at Corvallis, Oregon, which is further down dip (stations NEWP and

CORV, Figures 1 and 4). This observation is consistent with inferred shallowing of the plate coupling region as inferred by Hyndman and Wang [1993] and Mitchell *et al.* [1994]. Northern California continues to show the 11-month periodicity that was previously corroborated by tremor measurements [Szeliga *et al.*, 2004] and again the recurrence has continued after its original identification, with the most recent event occurring in October 2005.

[15] Nowhere in the Cascadia subduction zone is there evidence of longer-term transients such as seen along Japan's Nankai Trough, the Middle America trench offshore Mexico, or the Pacific subduction zone in Alaska [Larson *et al.*, 2004; Ohta *et al.*, 2006; Ozawa *et al.*, 2002] suggesting that something about the Cascadia subduction zone favors more frequent but smaller creep transients than other regions. For all Cascadia events, anomalous station offsets rarely exceed 10 d at any given station and 4–6 weeks networkwide. Moreover, cumulative surface deformation from transient creep rarely exceeds 5 mm, and no offsets exceed 6 mm, which is in stark contrast to the Nankai Trough and Middle America Trench, where several cm of transient deformation are observed [Larson *et al.*, 2004; Ozawa *et al.*, 2002].

4. Slip Distributions

[16] The growing density of GPS stations allows the distribution of slip from each transient to be formally estimated from GPS deformation. In this formulation, we specify the plate boundary surface by linearly interpolating between depth contours specified by Flück *et al.* [1997]. This surface is then divided into variable sized subfaults whose typical dimensions are around 25 km along strike and 15 km down dip. The exact dimensions of each subfault are variable depending on the geometry, which in the case of Cascadia is complex. The plate interface is far from planar, but exhibits a pronounced three-dimensional bend north of 47°N , changing strike from northeast to northwest. This translates into variable subfault strike changes of over 40° over less than one degree of latitude change and mandates that each subfault be independently specified with a unique local strike, dip and rake, in addition to its along-strike and down-dip length. The subfaults, as viewed from the vertical, are shown in Figure 8.

[17] Inverting for slip amounts to solving

$$Gs = d + \epsilon, \quad (7)$$

where G is a Jacobian matrix of Green's functions relating surface displacement to a unit of pure thrust fault slip, s is the vector of dip-slip slip at each subfault, d is the vector of north, east and vertical slow slip event offsets, weighted by their formal uncertainties, for each GPS station recording an event (Table 1), and ϵ is error. This matrix is severely underdetermined (G is $(M \times N)$, $M \ll N$), and additional information is required to reduce the nonuniqueness and aid in stabilizing the inversion process. We apply two constraints that are often utilized to help stabilize the solution of equation (7), positivity and solution smoothness.

[18] The first constraint, positivity, is achieved through solving for s in equation (7) with the nonnegative least squares algorithm of Lawson and Hanson [1995]. The

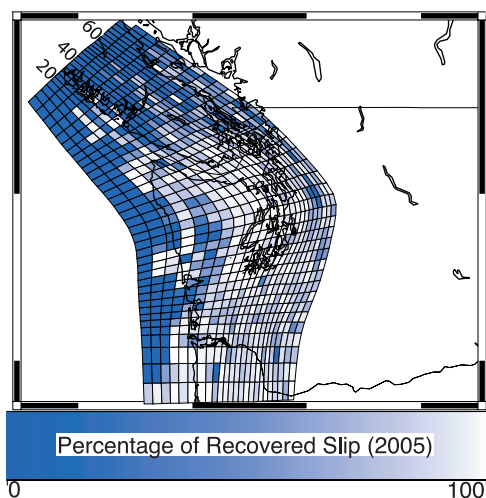


Figure 8. Resolution of slip along the plate interface from the Cascadia GPS geometry of early 2005, when roughly 30 continuous GPS stations were recording. Resolution is derived by computing the percentage of synthetic slip recovered on each subfault when corresponding synthetic deformation caused by slip on that subfault is inverted without smoothing. Resolution largely follows station distribution, with the highest resolution concentrated along the deeper plate interface where GPS stations concentrate and drops to zero offshore where no stations are located.

constraint that contains only nonnegative coordinates falls under the general category of linear least squares with linear inequality constraints. The problem of nonnegative least squares may be formally cast as minimizing $|Gs - d|$ subject to $s \geq 0$. The *Lawson and Hanson [1995]* algorithm converges in a finite number of steps and requires no explicit parameter selection by the user. Because of the complexity in the construction of the solution vector however, an explicit formula for formal covariance propagation has not been found. Thus while the algorithm may be used to formally invert deformation transients for slip, an accurate assessment of the covariances on the slip requires more complicated computation and is not presented here.

[19] The second constraint, smoothing, is often accomplished by augmenting the matrix with additional rows that encode a finite difference approximation of the Laplacian operator and augmenting the observation vector with an equal number of rows containing zeros. While the augmentation of the original problem with these two constraints does not entirely eliminate the problem of nonuniqueness, it does reduce the number of possible slip distributions. The introduction of the smoothing constraint, however, requires finding an optimum weighting factor to control the degree of smoothing. This weight is determined by cross validation.

[20] Cross-validation schemes involve repeatedly solving a data-reduced vector form of equation (7) and constructing a bootstrap estimate of the overall ability of the data set d to predict missing data subsets [*Efron and Tibshirani, 1994*]. “Leave-one-out” cross validation is one end-member of the cross-validation scheme where the data-reduced vector is formed by removing one data point at a time. Parameter estimation then proceeds by solving equation (7), using s to forward predict the removed data point, and recording the

squared misfit between the removed data and its predicted value. The removed data point is then replaced and a new data point is removed. For each smoothing parameter value, a sum of squared misfits metric may be calculated, with the minimum sum of squared misfit providing the optimal parameter. Figure 9 shows the trade-off between the smoothing coefficient and maximum inferred slip, which vary inversely with one another and cumulative moment, as a function of CVSS misfit.

[21] Figure 9, computed for the 2005 Cascadia network geometry, shows an obvious minimum CVSS misfit, but in general this will only occur for a sufficiently dense GPS network. Figure 9 also shows that despite the trade-off between smoothing and maximum inverted amplitude of slip, the inferred equivalent moment magnitude is invariant with respect to smoothing parameter chosen.

[22] Figure 8 shows a spatial estimation of slip resolution for the station geometry that existed for the September 2005 event. In a fashion analogous to the checkerboard resolution tests used to illustrate model sensitivity of seismic tomography, here we show inverted synthetic displacements for the 2005 geometry, employing the inversion methodology described above without smoothing. The resolution reaches 80% overlying regions of highest instrumentation but quickly falls way toward the trench and other areas far from instrumentation, reflecting the strong distance dependence of the near-field terms of the elastic Green’s functions. Figure 10 shows inverted slip distributions for the 12 largest events observed in Cascadia since 1997 that have 6 or more stations constraining transient deformation.

[23] The numbers of stations constraining the inversions range from 6 stations for the April 1997 event to 32 for the September 2005 transient. Typical magnitudes range from $M_w = 6.3$ for the smallest events to $M_w = 6.8$ for the largest observed in February–March 2003. Shown are inversions of the cumulative transient deformation for each event, which typically have average durations of 3–4 weeks, with the longest being 7 weeks and the shortest being 1 week.

5. Discussion

[24] The resolution of the GPS to infer details of slip is limited by a number of issues, and thus cannot be used to infer fine-scale details of faulting such as stress drop, for a number of reasons. The foremost problem traditionally has been station density, but with the rapid deployment of new instruments following the 2001 Nisqually earthquake within the subducting Juan de Fuca plate, the greater Puget basin region is well covered after early 2003. An additional limitation comes from the fact that Cascadia slip events generally do not produce resolvable vertical deformation, which proves to be the most useful in constraining the downdip extent of slip since the sense of motion (uplift versus subsidence) changes for slip at different depths. As a result, slip inversions of synthetic data are smeared prominently down dip, a feature apparent in the data inversions as well in Figure 10. This problem may also soon be resolved, however, since the increasing density of stations will, in the near future, allow stacking of nearby stations to extract vertical deformation. Finally, the elastic Green’s functions that map slip at depth to deformation at the surface are smooth, so that GPS cannot discriminate be-

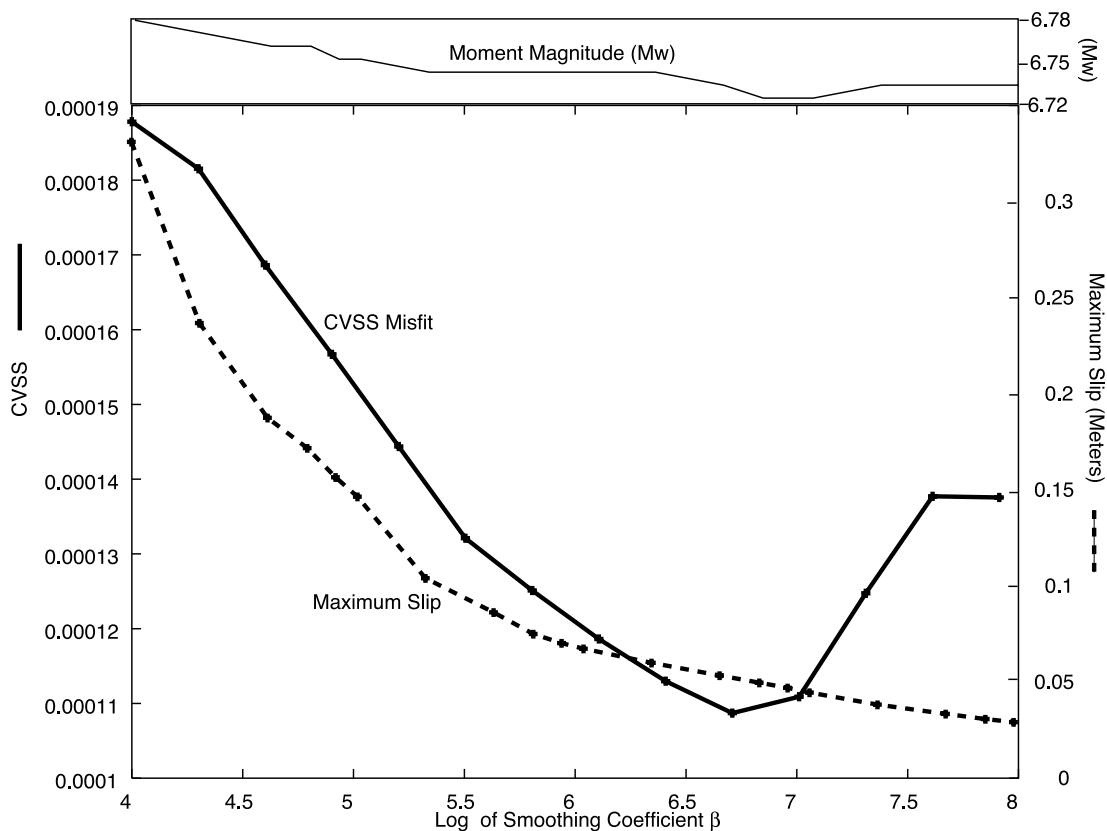


Figure 9. Selection of the optimum smoothing parameter is computed using cross-validation sum of squares (CVSS) misfit. For station geometries after 2003, CVSS misfit shows a pronounced minimum in misfit, which is selected for inversions shown in Figure 10. Maximum inferred slip trades off inversely with smoothing parameter β , but inferred moment magnitude is largely invariant with respect to smoothing parameter. For this reason, GPS cannot differentiate between the ensemble deformation caused by many small high stress drop slip events and a single broad, extremely low stress drop event.

tween the ensemble deformation caused by a large number of localized, high-stress drop events, and a single broad, low-stress drop creep transient. The slip inversions do, however, reliably assess total equivalent magnitude, as shown by Figure 9, and it is therefore worthwhile to systematically invert the largest creep events recorded on many stations for slip.

[25] Consistently found in the inversions is that the preponderance of slip takes place down dip of the 25-km depth contour on the subducting Juan de Fuca, and does not extend into the upper reaches of the plate interface. From a hazards standpoint, it is clear that none of the events recognized to date dissipate strain in the tightly coupled shallower plate interface, consistent with the findings of *Hyndman and Wang* [1993]. Insufficient time has yet passed to assess whether the slip observed along the lower reaches of the subduction zone bleeds off plate convergence strain as fast as it accumulates, which ultimately bears on the whether the deeper, slow slip region contributes to moment release during the eventual megathrust rupture.

[26] Laterally, many events extend to toward both the north and south, and are not obviously connected or disconnected through time. Throughout the Cascadia region instrumented to date, there are no obvious regions that lack slow slip events, only those that lack instrumentation. The

smallest events discernible with GPS take place in northwestern Oregon, but occasional smaller, aperiodic events take place elsewhere, most notably at the latitude of Seattle (47.5°N). These small events show roughly 1 cm of slip and equivalent moment magnitudes of $M_w = 6.3$, the smallest resolvable with GPS. The largest of the observed transients, by contrast, appear to slip a few centimeters along the plate interface between depth contours of 25 to 40 km along the subducting Juan de Fuca plate. Typical slip patch sizes for these events are estimated to be roughly 220 km along strike and 50 km down dip. At the current time, because of instrument density, it is not possible to invert for slip in Oregon or northern California.

[27] A consistent feature in all Cascadia events is that they are short lived and show relatively small transient deformation of less than 1 cm, unlike other subduction zones. This may generally reflect a slower rate of convergence in Cascadia than at other margins, or it may be symptomatic of as yet unknown properties along the plate interface. Far larger events, in terms of duration, spatial extent, observed deformation, and equivalent moment release, have been observed in many other regions, most notably the Middle America, Alaskan and Nankai subduction zones. An inferred 250 km \times 50 km segment along the Guerrero, Mexico seismic gap produced several centimeters

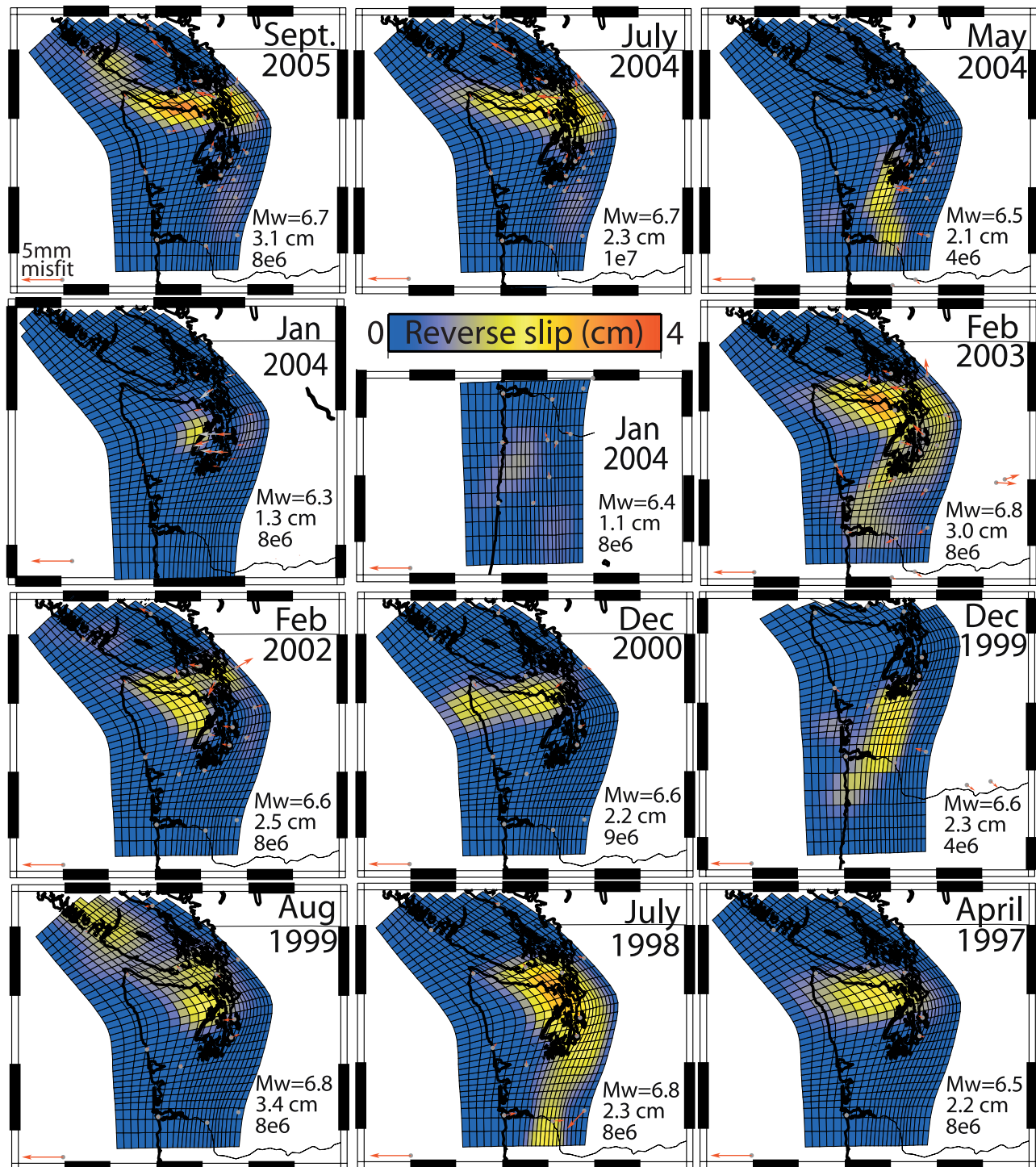


Figure 10. Slip distributions for Cascadia slow slip events are shown for the largest 12 events from the last decade. GPS-inferable moment magnitudes range from 6.3 to 6.8; events below $M_w = 6.3$ are not resolvable with GPS. Maximum inverted slip is 3.6 cm for all events, but this is strongly a function of the smoothing coefficient selected on the basis of the CVSS minimum misfit (Figure 9). Red vectors show misfit between data and vector offsets predicted by the slip distributions shown. Equivalent moment magnitude, maximum modeled slip, and smoothing weight that minimizes CVSS misfit shown for each inversion. See Figure 8 for depth contours.

of deformation and moment release equivalent to a $M_w = 7.3$ earthquake over a 3-month period [Kostoglodov *et al.*, 2003], while the 2001 Tokai, Japan, and Alaskan slow slip events both had durations on the order of years [Ohta *et al.*,

2006; Ozawa *et al.*, 2002, 2001]. With the ongoing densification of GPS stations in Cascadia, time will tell whether longer-term events are observed here as well.

[28] **Acknowledgments.** This research was supported by National Science Foundation grant EAR-0208214, U.S. Geological Survey NEHERP award 04HQGR0005, the National Aeronautics and Space Administration grant SENH-0000-0264, and Central Washington University. Pacific Northwest Geodetic Array (PANGA) data collection supported by the National Science Foundation under grants EAR-0318549 to UNAVCO, Inc. and EAR-0002066 and EAR-9616540 to CWU; by the National Aeronautics and Space Administration NASA contracts NAG5-13728 and NAG5-7672; and by the U.S. Geological Survey NEHRP Award 04HQAG0007 and Central Washington University. We thank the Western Canadian Deformation Array operated by the Pacific Geoscience Centre for the Geological Survey of Canada for use of their data. Wavelet transform figures were created using LastWave, available from <http://www.cmap.polytechnique.fr/~bacry/LastWave>.

References

- Blewitt, G. (1989), Carrier phase ambiguity resolution for the Global Positioning System applied to geodetic baselines up to 2000 km, *J. Geophys. Res.*, *94*, 10,187–10,203.
- Blewitt, G., and D. Lavallée (2002), Effect of annual signals on geodetic velocity, *J. Geophys. Res.*, *107*(B7), 2145, doi:10.1029/2001JB000570.
- Dong, D., P. Fang, Y. Bock, M. K. Cheng, and S. Miyazaki (2002), Anatomy of apparent seasonal variations from GPS-derived site position time series, *J. Geophys. Res.*, *107*(B4), 2075, doi:10.1029/2001JB000573.
- Dragert, H., K. Wang, and T. S. James (2001), A silent slip event on the deeper Cascadia subduction interface, *Science*, *292*, 1525–1528.
- Dragert, H., K. Wang, and G. Rogers (2004), Geodetic and seismic signatures of episodic tremor and slip in the northern Cascadia subduction zone, *Earth Planets Space*, *56*, 1143–1150.
- Efron, B., and R. J. Tibshirani (1994), *An Introduction to the Bootstrap*, CRC Press, Boca Raton, Fla.
- Flück, P., R. D. Hyndman, and K. Wang (1997), Three-dimensional dislocation model for great earthquakes of the Cascadia subduction zone, *J. Geophys. Res.*, *102*(9), 20,539–20,550.
- Golub, G., and C. Val Loan (1996), *Matrix Computations*, John Hopkins Univ. Press, Baltimore, Md.
- Hirose, H., K. Hirahara, F. Kimata, N. Fujii, and S. Miyazaki (1999), A slow thrust slip event following the two 1996 Hyuganada earthquakes beneath the Bungo Channel, southwest Japan, *Geophys. Res. Lett.*, *26*(21), 3237–3240.
- Hyndman, R. D., and K. Wang (1993), Thermal constraints on the zone of major thrust earthquake failure: The Cascadia subduction zone, *J. Geophys. Res.*, *98*, 2039–2060.
- Ide, S., D. R. Shelly, and G. C. Beroza (2007), Mechanism of deep low frequency earthquakes: Further evidence that deep non-volcanic tremor is generated by shear slip on the plate interface, *Geophys. Res. Lett.*, *34*, L03308, doi:10.1029/2006GL028890.
- Ito, Y., K. Obara, K. Shiomi, S. Sekine, and H. Hirose (2007), Slow earthquakes coincident with episodic tremors and slow slip events, *Science*, *315*, 503–506, doi:10.1126/science.1134454.
- Kao, H., S.-J. Shan, H. Dragert, G. Rogers, J. F. Cassidy, and K. Ramachandran (2005), A wide depth distribution of seismic tremors along the northern Cascadia margin, *Nature*, *436*(7052), 841–844.
- Kawasaki, I., Y. Asai, Y. Tamura, T. Sagiya, N. Mikami, Y. Okada, M. Sakata, and M. Kasahara (1995), The 1992 Sanriku-Oki, Japan, ultra-slow earthquake, *Journal of Physics of the Earth*, *43*(2), 105–116.
- Kostoglodov, V., S. K. Singh, J. A. Santiago, S. I. Franco, K. M. Larson, A. R. Lowry, and R. Bilham (2003), A large silent earthquake in the Guerrero seismic gap, Mexico, *Geophys. Res. Lett.*, *30*(15), 1807, doi:10.1029/2003GL017219.
- Langbein, J., and H. Johnson (1997), Correlated errors in geodetic time series: Implications for time-dependent deformation, *J. Geophys. Res.*, *102*(1), 591–603.
- Larson, K. M., A. R. Lowry, V. Kostoglodov, W. Hutton, O. Sánchez, K. Hudnut, and G. Suárez (2004), Crustal deformation measurements in Guerrero, Mexico, *J. Geophys. Res.*, *109*, B04409, doi:10.1029/2003JB002843.
- Lawson, C. L., and R. Hanson (1995), *Solving Least Squares Problems, Classics Appl. Math.*, vol. 15, Soc. for Ind. and Appl. Math., Philadelphia, Pa.
- Lowry, A. R., K. M. Larson, V. Kostoglodov, and R. Bilham (2001), Transient fault slip in Guerrero, southern Mexico, *Geophys. Res. Lett.*, *28*(19), 3753–3756.
- Mao, A., C. G. A. Harrison, and T. H. Dixon (1999), Noise in GPS coordinate time series, *J. Geophys. Res.*, *104*(2), 2797–2816.
- McCausland, W., S. Malone, and D. Johnson (2005), Temporal and spatial occurrence of deep non-volcanic tremor: From Washington to northern California, *Geophys. Res. Lett.*, *32*, L24311, doi:10.1029/2005GL024349.
- Miller, M., T. Melbourne, D. Johnson, and W. Q. Sumner (2002), Periodic slow earthquakes from the Cascadia subduction zone, *Science*, *295*, 2423, doi:10.1126/science.1071193.
- Miller, M. M., D. J. Johnson, C. M. Rubin, H. Dragert, K. Wang, A. Qamar, and C. Goldfinger (2001), GPS-determination of along-strike variation in Cascadia margin kinematics: Implications for relative plate motion, subduction zone coupling, and permanent deformation, *Tectonics*, *20*(2), 161–176.
- Mitchell, C. E., P. Vincent, R. J. Weldon II, and M. A. Richards (1994), Present-day vertical deformation of the Cascadia margin, Pacific Northwest, United States, *J. Geophys. Res.*, *99*, 12,257–12,277.
- Nikolaïdis, R. M. (2002), Observation of geodetic and seismic deformation with the Global Positioning System, Ph.D. thesis, Univ. of Calif., San Diego.
- Obara, K. (2002), Nonvolcanic deep tremor associated with subduction in southwest Japan, *Science*, *296*, 1679–1681.
- Ohta, Y., J. T. Freymueller, S. Hreinsdóttir, and H. Suito (2006), A large slow slip event and the depth of the seismogenic zone in the south central Alaska subduction zone, *Earth Planet. Sci. Lett.*, *247*, 108–116.
- Ozawa, S., M. Murakami, and T. Tada (2001), Time-dependent inversion study of the slow thrust event in the Nankai trough subduction zone, southwestern Japan, *J. Geophys. Res.*, *106*, 787–802.
- Ozawa, S., M. Murakami, M. Kaidzu, T. Tada, T. Sagiya, Y. Hatanaka, H. Yurai, and T. Nishimura (2002), Detection and monitoring of ongoing aseismic slip in the Tokai region, central Japan, *Science*, *298*, 1009–1012.
- Rogers, G., and H. Dragert (2003), Episodic tremor and slip on the Cascadia subduction zone: The chatter of silent slip, *Science*, *300*, 1942–1943.
- Royle, G. T., A. J. Calvert, and H. Kao (2006), Observations of non-volcanic tremor during the northern Cascadia slow-slip event in February 2002, *Geophys. Res. Lett.*, *33*, L18313, doi:10.1029/2006GL027316.
- Shelly, D. R., G. C. Beroza, S. Ide, and S. Nakamura (2006), Low-frequency earthquakes in Shikoku, Japan, and their relationship to episodic tremor and slip, *Nature*, *442*, 188–191, doi:10.1038/nature04931.
- Szeliga, W., T. I. Melbourne, M. M. Miller, and V. M. Santillan (2004), Southern Cascadia episodic slow earthquakes, *Geophys. Res. Lett.*, *31*, L16602, doi:10.1029/2004GL020824.
- Torrence, C., and G. P. Compo (1998), A practical guide to wavelet analysis, *Bull. Am. Meteorol. Soc.*, *79*(1), 61–78.
- Zumberge, J. F., M. B. Hefflin, D. C. Jefferson, M. M. Watkins, and F. H. Webb (1997), Precise point positioning for the efficient and robust analysis of GPS data from large networks, *J. Geophys. Res.*, *102*, 5005–5017.

T. Melbourne, M. Miller, and M. Santillan, Department of Geological Sciences, Central Washington University, 400 E. University Way, Ellensburg, WA 98926, USA.

W. Szeliga, Department of Geological Sciences, University of Colorado, 2200 Colorado Avenue, CB 399, Boulder, CO 80309-0399, USA. (szeliga@colorado.edu)